Subpicosecond Pump−Supercontinuum Probe Spectroscopy of LH2 Photosynthetic Antenna Proteins at Low Temperature

A. Freiberg,*,†,‡ J. A. Jackson,† S. Lin,† and N. W. Woodbury†

Department of Chemistry and Biochemistry and Center for the Study of Early Events in Photosynthesis, Arizona State University, Tempe, Arizona 85287, and Institute of Physics, University of Tartu, EE2400 Tartu, Estonia

Received: October 30, 1997; In Final Form: April 2, 1998

Exciton relaxation and energy-transfer processes in the B850 circular aggregate of bacteriochlorophyll *a* molecules from the purple nonsulfur photosynthetic bacterium *Rhodobacter sphaeroides* were studied at temperatures below 18 K. Excitons were selectively excited by a 7 nm spectral bandwidth pump pulse resonant with the inhomogeneously broadened long-wavelength side of the B850 ground-state absorption spectrum (between 860 and 879 nm). The transient spectra were measured over the 786−924 nm spectral range using a white light continuum probe pulse. Characteristic changes of transient spectra were observed over 4 decades of time, from about 10^{-13} to about 10^{-9} s. The spectral evolution was pump wavelength-dependent, changes being least notable at far-red excitation. A simple model was put forward to interpret the data, assuming that the sample consists of an ensemble of spectrally disorded excitons, each representing a separate B850 ring. It was found that the exciton coupling and diagonal disorder play almost equally important roles in the formation of the spectral and dynamical properties of light excitations in B850 antenna. The main effects of disorder considered were the spectral shifts, splitting of the degenerate exciton levels, and redistribution of the dipole strength of the transitions. Assuming that the contribution of least disturbed excitons is largest near the peak of the ground-state absorption spectrum and greatest near the edge, most of the known spectroscopic properties of LH2 complexes can be well understood, at least qualitatively. Specifically, the rough 100 fs response time was assigned to interexciton level relaxation; the three time constants, ca. 800 fs, ca. 15 ps, and ca. 150 ps, were attributed to exciton energy transfer, most likely, between the B850 rings. The ca. 1 ns decay time is due to the finite exciton lifetime. The circular LH1 antennas likely possess similar properties.

1. Introduction

In photosynthetic membranes, the antenna pigment−protein complexes serve to carry out very efficient light energy collection, transfer, and concentration into the photochemical reaction center. Despite intensive study, the precise nature of the excited states of the pigments involved and the role of the protein moiety in governing the dynamics of the excited states are still under debate. More sophisticated analysis of this system has been catalyzed by recent crystallographic data,[1−3] which have demonstrated that the core (LH1) and peripheral (LH2) antenna units have a simple ringlike structure in purple photosynthetic bacteria. The LH2 accommodates two rings of bacteriochlorophyll *a* (BChl) molecules, B800 and B850 (labeled according to the long-wavelength Q_y absorption band maxima, which are, as seen in Figure 1, at about 800 and 850 nm, respectively). The B850 ring includes 18 (or 16, depending on the species) BChl molecules in a tilted face-to-face or water-wheel-like arrangement. B800 is, correspondingly, an array of 9 or 8 BChls in a side-by-side arrangement.

There is at present a general understanding that the electronic excitations in the B850 and B875 (LH1) rings are at least to some extent delocalized, even at room temperature. The resulting exciton states are properties of a molecular group, not a single molecule. The structural basis of this viewpoint is the very dense packing of the BChl molecules in the B850 and B875 arrays which have a center-to-center distance of less than 1 nm and a transition dipole geometry favoring strong dipole−dipole coupling.[4−7] The situation is generally different in the B800

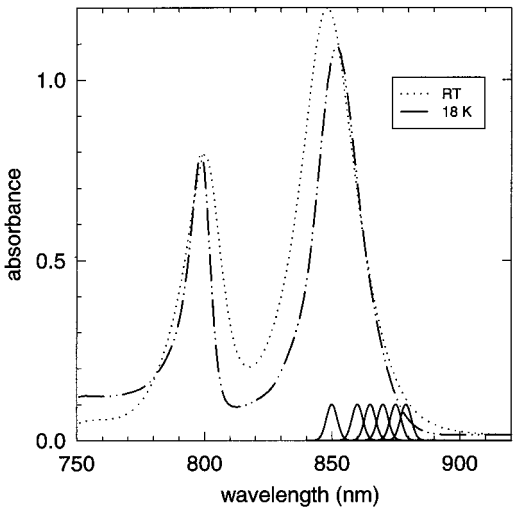

Figure 1. Steady-state absorption spectra of LH2 chromatophores at room temperature (dotted curve) and at 18 K (dash−dotted curve). Superimposed are the Gaussian shape spectra of the pump pulses of 7 nm bandwidth with the peak at the excitation wavelengths applied in the present work (850, 860, 865, 870, 875, and 879 nm).

* To whom correspondence should be addressed. E-mail freiberg@fi.tartu.ee; phone +372-7-383024; Fax +372−7−383033.
† Arizona State University.
‡ University of Tartu.

S1089-5639(98)00028-0 CCC: $15.00
Published on Web 05/14/1998

ring. There the distance between adjacent B800 molecules is over 2 nm, coupling is about an order of magnitude weaker,[4] and the excitations are considered more or less localized initially on a single B800 molecule.

A consensus is lacking, however, when the exciton coherence sizes, energy level structure, energy transfer, and relaxation properties in the B850 and B875 rings are considered. Both theoretical and experimental arguments have been raised, supporting a wide variety of possible exciton coherence sizes in the B850 aggregate at room temperature covering 2,[8−12] 2−3,[13] 3−4,[14] 4 ± 2,[15] 12,[16] 16 ± 4,[17] and the whole ring of 18[4,5,18−24] BChl molecules. In one limit, the dynamics of excited states and energy transfer is viewed as a rapid localization of the excitation energy on the BChl dimers. Subsequent energy transfer takes place by an incoherent mechanism.[10,12,14,25−27] In another limit, the excited electronic states are extensively delocalized, and coupling to the vibrations leads to the scattering between the quasistationary exciton states.[4,5,17,18,21] Specifically, steady-state exciton superradiance measurements have demonstrated[14] that lowering temperature from room temperature to 4 K more than doubles the size of the exciton in the LH1 antenna complexes. This is what one would normally expect since phonons lead to exciton localization and the density of phonons decreases with temperature. However, in the LH2 B850 ring the exciton coherence size seems to remain small and equal to about three BChl molecules irrespective of temperature.[14] This may be an indication of a fast (relative to the exciton lifetime) exciton localization dynamics that may be apparent in time-resolved studies. The hole burning data of *Rb. sphaeroides* LH2[22,23,29] have been evaluated in terms of a weakly disordered aggregate. The analysis performed in ref 23 concluded that the lowest exciton levels, characterized by narrow holes with full width at half-maximum (fwhm) equal to 3.2 cm^{-1} at 4.2 K, are distributed over a band (denoted as B870) with a fwhm of about 60 cm^{-1}. The peak of the B870 band was found to be roughly 260 cm^{-1} below the B850 absorption maximum. According to more recent data,[22,29] the B870 bandwidth is twice as large, about 120 cm^{-1}, and closer to the B850 band maximum (185 cm^{-1} below the maximum). The new parameters have been explained by improved sample quality. The very broad (fwhm of about 210 cm^{-1}) blue sideband accompanying the narrow holes was assigned to higher exciton state(s), broadened due to ultrafast downward energy relaxation.[23] The width of the narrow hole was attributed to the dephasing of the exciton transition energy.

Some of the discrepancies between different measurements may be a consequence of different definitions of the exciton size and other parameters, as addressed previously.[10,14,27] Another reason may be that the theoretical models used to date are grossly oversimplified. A minimum set of interactions that a realistic model needs to consider should include, in addition to excitonic coupling between the pigment transition moments, the coupling between pigments and their surroundings. The pigment−pigment and pigment−protein interactions combined are responsible for the specific monomer transition energies and for the static diagonal disorder that leads to an inhomogeneous broadening of the spectral lines. The exciton−phonon and exciton vibrational couplings determine the dynamic properties of excitons and their homogeneous spectral line shapes. The spectral disorder and the temperature-dependent exciton−phonon coupling are both factors that lead to localization of excitons. The extent of localization depends on relative values of the relevant coupling parameters. A wide range of estimates for these parameters exists. For instance, resonance interaction energies between 100 and 806 cm^{-1} and inhomogeneous site distribution widths between 0 and 527 cm^{-1} have been assumed.[4,5,10−24,27] A theoretical arsenal, capable of dealing with all the appropriate interactions in a single model, is still in its infancy.[28] The fact that some techniques are more sensitive to certain aspects of the phenomena under study than the others aside, the particular parameters and their relative importance also depend on experimental conditions, such as temperature, how the nonstationary initial state is prepared, and the sample quality.[22]

It is our belief that rigorous understanding of many of the energetic and dynamic aspects of light excitations in the antenna proteins is still lacking. In a hope of gaining new insight into the problem, the present experimental study of exciton dynamics in the B850 ring of the LH2 antenna was undertaken. The following distinctive aspects of our investigation should be underlined. (i) A subpicosecond transient absorption technique with spectrally narrow pump pulses has been used. The pump pulse spectral bandwidth (fwhm) was 6.5−7.0 nm ($\Delta\nu$ = 84−92 cm^{-1}), depending on the center wavelength, which is significantly smaller than the fwhm of the B850 steady-state absorption band (275 cm^{-1} at 18 K, see Figure 1). $\Delta\nu$ is also less than the assumed transition dipole−dipole (exciton) interaction energy between the BChls in the B850 ring (see above) and the recent estimates[4−7,22,23,29] of the zero-order energy gap (about 150 cm^{-1}) between the two lowest $k = 0$ and $k = \pm 1$ exciton levels of the B850 ring (see Discussion). (ii) The excitation pulses have been tuned over the red-side slope of the B850 ground-state absorption band in order to prepare the system in a specific exciton level or superposition of the levels. (iii) Measurements have been performed at low temperature ($T \leq 18$ K) in order to reduce the homogeneous spectral bandwidth compared both to the exciton coupling energy and to the inhomogeneous spectral broadening. (iv) Chromatophores of mutant membranes of *Rhodobacter (Rb.) sphaeroides* that include only LH2 antenna proteins and are devoid of the core LH1 antenna and reaction center proteins[31] have been studied. This has eliminated the possible sample quality problems caused by the protein isolation procedure and usage of detergents.

Femtosecond time-resolved spectral studies of B850 excitons at liquid helium temperature have been reported earlier.[15,30] However, different from our experiment, a broadband (≈300 cm^{-1}) and nonresonant excitation at 800 nm has been used.

2. Experimental Section

Isolation of Chromatophores and Sample Preparation. Cultures of a *Rb. sphaeroides* strain with deletions in the *puf* operon containing the LHI and core reaction center genes were grown semiaerobically in a rich medium as previously described.[31] After harvesting, the cells were resuspended in TEN (15 mM Tris-HCl, pH 8, 1 mM EDTA, 0.1 M NaCl), and the cells were lysed at 20 000 psi in a French pressure cell. The cell extracts were incubated with DNAse and then centrifuged at low speed (8000 rpm, 30 min, Sorvall GS3 rotor) to remove whole cells and debris. The membranes were isolated by high-speed centrifugation (25 000 rpm, 2 h 45 min, Beckman Ti45 rotor) on a 0.3, 0.6, 1.2 M sucrose step gradient containing TEN. The chromatophore preparations were stored at −75 °C in 15% (v/v) glycerol.

All samples were suspended in a TEN buffer at pH 8.0, giving a final optical density of about 20 in a 1 cm cuvette at 850 or 875 nm. The protein solution was further diluted with glycerol

(in a 1:2 buffer/glycerol volume ratio), fixed between the two fused quartz plates about 1.2 mm apart, and slowly cooled in a coldfinger type temperature-controlled cryostat (Air Products). The optical quality of the samples at low temperatures is a concern because of usual sample cracking upon cooling below 130−140 K and of resulting severe scattering of the laser beams. As described previously,[32] this problem can readily be overcome by coating the inner surfaces of the sample cell plates by Repel-Silane (a solution of dimethyldichlorosilane in trichloroethane). In addition, samples were degassed and freshly prepared sample material was used. This resulted in a roughly 4 cm^2 sample surface area with few cracks and thus minimal scattering of the excitation beam. Because of this, it was possible to perform absorbance change measurements across the spectral region of excitation without scattering artifacts.

Femtosecond Pump−Probe Setup. The femtosecond transient absorption spectrometer has been described earlier.[33,34] A 70 ps pulse from the mode-locked Nd:YAG laser was compressed in a fiber compressor, frequency doubled, and used to pump a rhodamine 6G dye laser (Spectra Physics). The output pulses from the dye laser at 590 nm were further compressed and then amplified in a regenerative amplifier (Continuum) operating at 540 Hz. The resulting roughly 200 μJ and 150 fs pulse was split into two parts. One portion was used to generate a continuum in a 1.2 cm rotating quartz plate. This continuum pulse was passed through a 6−7 nm band-pass interference filter to select the specific excitation wavelengths used (see Figure 1). Fine-tuning of the excitation wavelength was achieved by tilting the filter in the laser beam. These pulses were then reamplified by a prism dye amplifier (Santa Ana) and used as the excitation pulses in the pump−probe experiment. The dye amplifier was in turn pumped by the 540 Hz regenerative amplifier. The other portion of the original 200 μJ pulse was used to generate a spectral continuum in a 1 cm flowing water cell from which the probe and reference beams were formed. A stepping motor driven delay line controlled the variable time delay between the pump and probe/reference pulses. The sample transmission spectra at probe (p) and reference (r) channels, $T_{p,r}(\lambda,t)$, were analyzed by a 0.275 m single-grating spectrograph (Acton Research) equipped with a dual diode array detector (Princeton Instruments). The optical density (absorbance) spectra at different time delays, t, were calculated as

$$\Delta OD(\lambda,t) = \log(T_r/T_p) \qquad (1)$$

The time-resolved absorption difference spectrum is defined as the difference between the delayed optical density spectra of the sample perturbed by the pump pulse and of the unperturbed sample.

The sensitivity limit of our spectrometer for the spectral measurements was about $\pm 5 \times 10^{-4}$ OD units and about $\pm 1 \times 10^{-3}$ units for the kinetics measurements. The pump bandwidth-limited time resolution of the setup was about 200 fs. Each kinetic trace was divided into 100 points. Various scanning lengths between 3 and 900 ps were utilized in order to trace both fast and slow relaxation phases. At each delay time the result of 1080 laser shots was collected and averaged. Many (up to 20) scans were usually collected and averaged in order to obtain a satisfactory signal-to-noise ratio. The pump and probe beam polarization were kept at the "magic angle", 54.7°. The spectral band-pass used in the present measurements was 2 nm over the 130 nm (786−924 nm) spectral range probed.

The intensity of the weakest pump pulses used was about 100 μJ/cm^2, corresponding to a photon density of about 4×10^{14} quanta/cm^2 per pulse at 860 nm. Along with a relatively low 540 Hz pulse repetition rate, this is a sufficiently low intensity to avoid any essential distortion of the data by the multiple excitation effects, such as singlet−singlet or singlet−triplet annihilation. No significant changes of the spectra and temporal behavior of the kinetics were observed when checking with 3 times more intense pump pulses. The probe pulse intensity, counted per unit spectral interval, was maintained several orders of magnitude less than the pump pulse intensity.

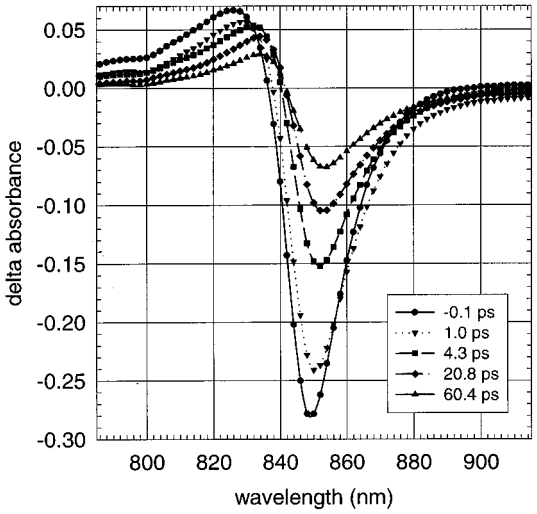

Figure 2. Pump−probe spectra at room temperature at several indicated probe pulse time delays. Time zero is defined at the maximum of the bleaching peak. Excitation with about 150 fs pulses at the ground-state absorption maximum (850 nm) is used. The spectra are recorded with a resolution of 2 nm per channel.

Data Analysis. The data were analyzed by using a SigmaPlot 4.0 for Windows (Jandel Inc.) package and a home-written global analysis routine based on the MATLAB program from Mathworks.

3. Results

Spectra. Figure 2 presents transient differential absorption spectra of the LH2 complexes recorded at room temperature. Different probe light delay times between −0.1 and 60.4 ps have been used. Time zero has been defined as the point at which the negative (bleaching) signal reaches its maximum. The sample has been excited at 850 nm, the peak of the ground-state absorption spectrum.

At delay times longer than the width of the pump and probe pulse cross-correlation function, the coherent coupling artifacts can be ignored. Then the differential absorption spectrum may be considered as a sum of three quasi-independent pump pulse-induced processes: excited-state absorption (ESA), stimulated emission (SE), and ground-state bleaching (GSB). From those the contributions of GSB and SE have a negative sign in Figure 2 (creating a bleaching signal), and the contribution of ESA has a positive sign. As seen, the spectra in Figure 2 appear to be rather similar to the earlier reported transient absorption spectra.[15,21] We note in passing that, in ref 15, 100 fs pump pulses centered at 800 nm and, in ref 21, 35 fs pulses centered at 850 nm have been used. Very similar spectra have also been reported for the LH1 antenna.[19,25]

The initial bleaching in Figure 2 appears at the excitation pulse center wavelength. A few nanometers red shift of the entire spectrum (best seen at the zero-crossing point around 840 nm) then follows until about 10−20 ps past the pump pulse. The signal decay and broadening of the negative part of the spectrum accompany the spectral shift. (Simultaneously, a

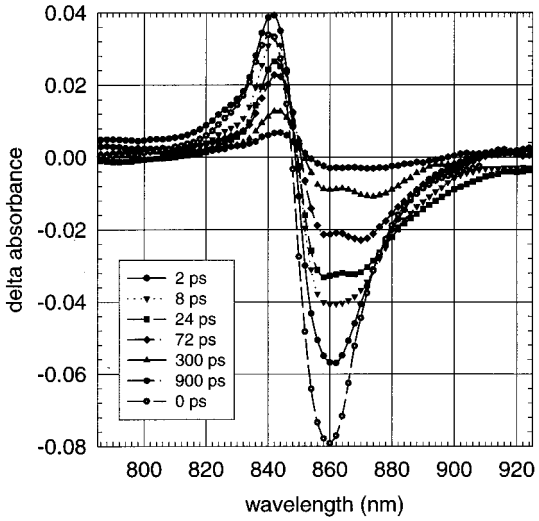

Figure 3. Pump−probe spectra excited at 865 nm and 16 K. Other conditions are as in Figure 2.

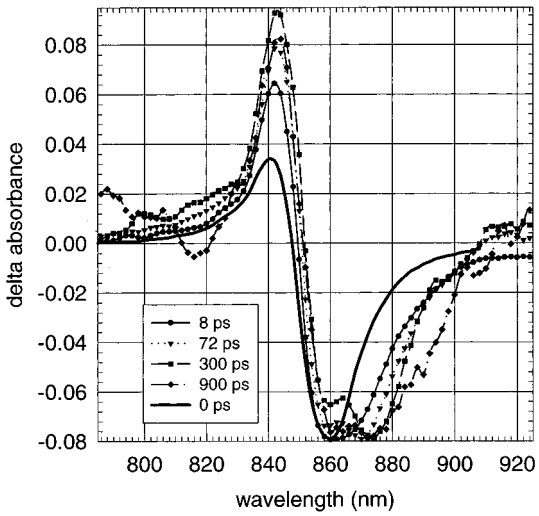

Figure 4. Spectra from Figure 3 normalized with respect to the bleaching maximum at zero time (the zero time spectrum is highlighted with bold solid curve).

narrowing of the positive signal is observed.) The decay of the signal is not monoexponential. In the LH1 antenna of *Rhodospirillum rubrum*, similar spectral dynamics has been recorded,[25] but the spectral changes were faster and only observable in the subpicosecond time range.

Figure 3 shows the transient absorption spectra of LH2 at 16 K, as excited at 865 nm (about 176 cm^{-1} below the maximum of the B850 absorption band at 852 nm, see Figure 1). There are several notable differences in Figure 3, compared to the room-temperature data of Figure 2:

(i) The whole spectrum is shifted to the red. This can only partially be a result of a few nanometer red shift of the ground-state absorption spectrum caused by lowering temperature (see Figure 1). At longer delay times, the transient absorption spectrum extends well beyond the long-wavelength edge of the steady-state absorption spectrum that is at about 890 nm. Considering the known low-temperature steady-state fluorescence emission peak of LH2 at about 880 nm,[35] it is probably reasonable to assume that the contribution of SE into the differential absorption spectrum is substantial at wavelengths longer than 880 nm.

(ii) The initial bleaching appears not at the excitation pulse center wavelength, but about 4−5 nm to the blue from it. Like at room temperature, the initial bleaching spectrum is narrow, almost of the same width as the steady-state absorption spectrum. The spectrum broadens considerably within a picosecond or two. This broadening, however, is strongly asymmetric, only toward long-wavelength side, and proceeds much slower than the spectrum at room temperature. At low temperature, the time evolution of the spectrum can be observed over almost 4 decades of time. Most remarkably, at about 10 ps, a gradual splitting of the bleaching peak into two resolved spectral components sets in. Of the two, only the long-wavelength component appears to continue red shifting. Though its amplitude diminishes, the short-wavelength component seems to remain almost at the same position. At the 900 ps delay (the longest applied), the two peaks are separated by about 14 nm (182 cm^{-1}). Note that during the same period the shift of the zero-crossing point near 850 nm is only about 5 nm and that of the positive peak even less, 2−3 nm.

(iii) The intensity ratio of the positive and negative parts of the spectrum in Figure 3 is much bigger than that in Figure 2. Figure 4, where the spectra of Figure 3 are normalized at the bleaching peak, shows that this ratio also gains intensity with time.

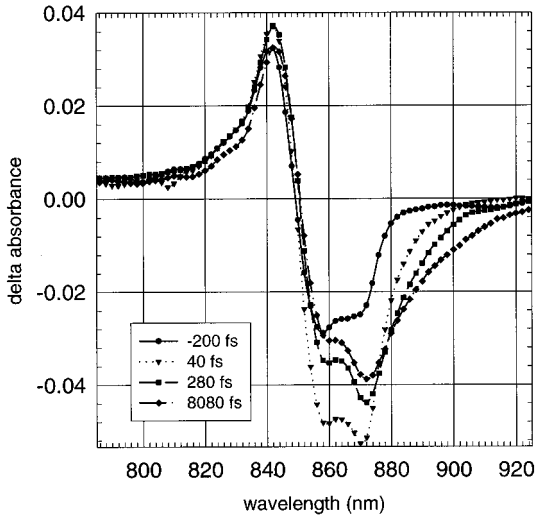

Figure 5. Short-time pump−probe spectra using 875 nm excitation. The temperature is 18 K.

Figure 4 shows normalized difference spectra and provides a better comparison of the bleaching band shapes at different delay times. With time, the long-wavelength bleaching peak becomes stronger relative to the short-wavelength one. Also, the slow spectral evolution is very evident when spectra measured with long delays are compared.

Figure 5 displays short-time transient absorption spectra using a longer wavelength 875 nm excitation (about 309 cm^{-1} below the maximum of the B850 steady-state absorption band). A few differences are apparent when spectra at similar delays are compared using different pump wavelengths (Figures 3 and 5). With the 875 nm excitation:

(i) The broad bleaching spectrum, similar to the later-time shape of the spectrum using 865 nm excitation, is observed initially. The bleaching spectrum again appears to be shifted to the blue from the excitation pulse center, but the low-energy bleaching peak seems to be slightly closer to the excitation wavelength.

(ii) The temporal red shift of the bleaching spectrum is much smaller. Within 80 ps the low-energy bleaching peak red shifted by only about 3 nm (data not shown). As can be seen in Figure

3, with 865 nm excitation the shift is at least 3 times larger during the same period. In Figure 5, there is still some intensity redistribution between the bleaching peaks going on in favor of the low-energy component.

(iii) The emergence of an extra, fairly broad bleaching/SE band from behind the major redmost bleaching peak, seen also in Figure 3, is now more evident. Red-shifting of this band smoothes out the long-wavelength slope of the bleaching spectrum, which initially was remarkably sharp. The red-shifting of the new band has been observed up to 200 ps (the longest delay time used in this series of experiments, data not shown), but it probably continued beyond that limit.

(iv) The intensity of ESA relative to GSB/SE component is stronger in Figure 5 compared to Figure 3.

Both Figure 3 and Figure 5 reveal a shoulder at 14−16 nm to the blue from the main ESA peak as well as a few feeble wiggles almost buried into the noise at even higher energy. The extra structure does not seem to change with time in Figure 5, whereas in Figure 3, it shifts to the red, in correlation with the GSB/SE spectrum. Considering its behavior, the structure could have a vibronic origin, reflect spectral heterogeneity, or represent an internal structure of the spectrum. We shall later show that it most probably represents an internal structure of the spectrum.

Kinetics. The kinetics of a few characteristic spectral components is presented over a 9 ps delay time scale in Figure 6. Figure 6a shows the data obtained using 865 nm excitation and that of Figure 6b, using 875 nm excitation. In both cases, the kinetics measured at the maximum of the GSB/SE band (at 860 nm with 865 nm excitation and at 872 nm with 875 nm excitation, respectively) demonstrates an initial pump pulse-limited decay, which is followed by a slower signal decline. By careful examination of the 872 nm kinetics in Figure 6b, one can discover a slight increase of the bleaching just after the initial drop before the decline takes over. The signal recorded at the long-wavelength edge of the GSB/SE spectrum (e.g., at 890−892 nm in Figure 6) is delayed compared to the almost instantaneous rise at shorter wavelengths. Kinetics recorded in the ESA region also depend on the probe wavelength. There is an initial fast decay when measured at the shoulder region and almost no change when measured at the peak of ESA. However, the most remarkable feature of Figure 6 is that the relative (compared to the peak value of the signal) amplitude of the initial decay changes when pump wavelength is changed. With 865 nm excitation the signal drops by about 25%, whereas the loss is only about 10% with 875 nm excitation. Using 860 nm excitation the initial drop is even larger, almost 40% (data not shown). Considering the possible origin of the initial ultrafast kinetics, it is important to realize that it is spectrally well separated from the excitation light, which essentially rules out the possibility that the phenomenon might be connected to an excitation coherent artifact.

The dispersion-corrected kinetics was analyzed using a global fitting routine. In the 9 ps scan length, the fitting returns 200 fs, 800 fs, and 38 ps time constants. For different, but understandable reasons, the first and the last time constants should be considered approximate. Fitting in the 100 ps time scale gives a subpicosecond component plus about 15 and 150 ps time constants. Additionally, a roughly 1 ns time constant can be found when fitting data taken over a longer time period. Summarizing, the kinetics in the transient absorption spectra of LH2 over the 790−920 nm spectral range can be characterized by five time constants: (sub-) 100 fs, 800 fs, 15 ps, 150 ps, and 1 ns. Note that all these time constants are in different orders of magnitude and therefore, in principle, well separable.

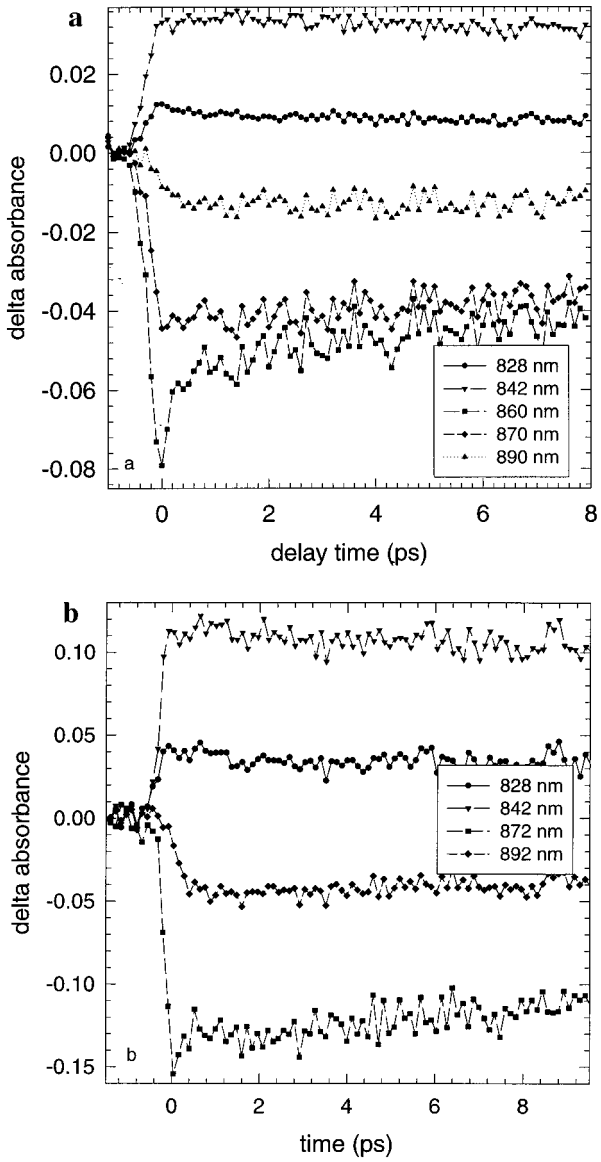

Figure 6. Directly measured (without dispersion correction) short-time absorbance change kinetics probed at the indicated wavelengths: (a) using 865 nm excitation; (b) using 875 nm excitation. The temperature is 16 K.

Depending on the recording wavelength, the time constants appear as signal decay or signal rise (lag). The given estimates of decay/rise parameters are in reasonable agreement with earlier time-resolved low-temperature results.[15,30,36−40] Specifically, the roughly 15 and 150 ps time constants were first resolved by the time-resolved fluorescence technique in LH1 chromatophores and antenna proteins.[36−39]

We finally point out that additional data, which have been gathered using 860, 870, and 879 nm excitation, are complementary and support the experimental data demonstrated in Figures 3−6.

4. Discussion

Excitons in Disordered Circular Arrays of Molecules. First, consider the properties of optical excitation in an idealized ringlike aggregate of N identical two-level molecules coupled to each other.[4,5,7,23] The intermolecular coupling makes the individual molecular excitation nonstationary and leads to a splitting of the N degenerate molecular levels into a band of N discrete one-exciton levels. The delocalized one-exciton level

energies can be calculated as[5]

$$E_k = E_0 - 2V\cos(2\pi k/N) \quad (2)$$

where E_0 is the localized (monomer) excitation energy, V is the coupling energy between the molecules, and k takes N integer values (for N even, $k = 0, \pm1, \pm2, ..., \pm N/2 - 1, N/2$; for N odd, $k = 0, \pm1, \pm2, ..., \pm(N - 1)/2$). As can be seen from eq 2, most of the levels in the band are 2-fold degenerate. The one-exciton bandwidth is roughly 4 times the intermolecular coupling energy. Due to intermolecular coupling also two-exciton, three-exciton, etc., up to N-exciton bands are created, according to the number of excitons in the aggregate.[41] However, optical transitions are only possible between the bands differing by a single exciton.

The ring of B850 molecules is constructed from nine α, β polypeptide pairs, each of which bind a pair of coupled BChl molecules.[1] The BChls from the neighboring polypeptide pairs couple with a slightly different energy.[4] The Q_y transition dipoles of individual molecules are tangential to the ring and are almost antiparallel within each dimer.[1] Due to the geometrical constraint, only the lowest energy exciton component of the elementary dimer carries essential absorption intensity,[4] and the B850 exciton spectrum may be described by a circular array of nine head-to-tail oriented transition dipoles almost in the plane of the ring.[7] It was shown earlier[4−7] that if all molecules were identical and their Q_y transition dipoles were oriented as was determined in ref 1, the transition to the lowest ($k = 0$) exciton state would carry less than 1% of the total oscillator strength. Most of the oscillator strength in this case would be concentrated into the two next lowest ($k = \pm1$) degenerate transitions. If this were the case, it should result in a substantial decrease in radiative rate constant at low temperature. As was emphasized in ref 14, this decrease was not observed. One may conclude that the model described is oversimplified and not consistent with the experimental facts in the B850 aggregate.

Several early experiments have suggested that the purple bacterial antenna may be spectrally heterogeneous.[42−44] However, biochemical evidence to support a large-scale spectral heterogeneity was and still is absent. An observation of a time-dependent red shift of the low-temperature fluorescence spectrum of chromatophores and isolated LH1/LH2 complexes[36−39,45,46] suggests that due to microscopic differences in the surroundings of antenna pigments (or pigment aggregates), the antenna spectra may be inhomogeneously broadened. That is, transition energies may be more or less continuously distributed over a broad spectral region. Perhaps most convincingly the existence of spectral inhomogeneity in chromatophores and antenna complexes was shown by spectral hole-burning experiments.[22,23,29] As will be discussed below, the present pump−probe data can only be understood, if substantial inhomogeneous broadening of the spectra is assumed.

Taking the spectral inhomogeneity or diagonal disorder (the latter term is customarily used in the solid-state physics literature) into account, the idealized exciton model of circular molecular aggregate described above has to be modified as follows (see refs 5−7 10, 14, 22, 23, and 27 for details). (i) All exciton levels will shift. This may be a blue or red shift, depending on the perturbation, but in the lowest-order approximation of the perturbation theory, the shift is uniform for all exciton levels and equal to Δ/N (assuming that the antenna homogeneity is disturbed at a single site by shifting the site energy by Δ). (ii) The degeneracy of the exciton levels will be removed, and the levels will be separated by $2|\Delta/N|$. One of the consequences of the level splitting is, for example, that the energy gap between the $k = 0$ and $k = -1$ levels will decrease with increasing disorder. (iii) With increasing disorder also the lowest energy $k = 0$ exciton state will become progressively more dipole allowed due to mixing with the $k = \pm1$ states. In the first order, the dipole strength of the transition to the lowest state will increase as $2(d_1|\Delta/N|/(E_1 - E_0))^2$. Here d_1 is the dipole moment of the $k = \pm1$ transition, and $E_1 - E_0$ is the energy gap between the $k = \pm1$ and $k = 0$ levels.[5] The dipole strength of higher, $k > \pm1$, transitions increases as $(2d_1|\Delta/N|/(E_k - E_1))^2$. Note that the energy gap, $E_k - E_1$, is different from the previous case.

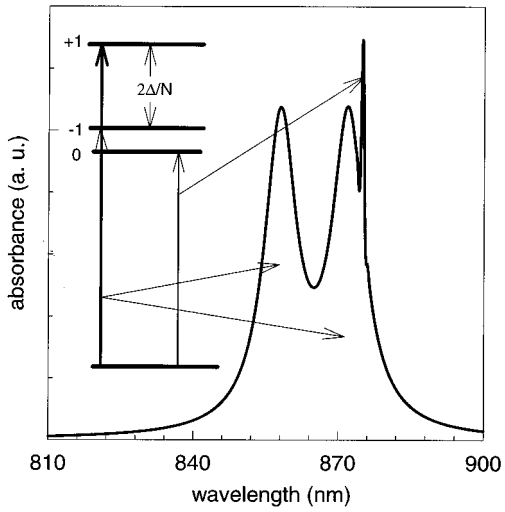

Figure 7. A model shape of the absorption spectrum of a hypothetical disordered exciton and the exciton level scheme. See text for explanations.

An expected shape of the absorption spectrum of a hypothetical disordered circular exciton ($N = 9$, transition dipole in the plane of the circle) is shown in schematic Figure 7, along with the exciton level scheme. Only the three lowest exciton levels and transitions are presented. The exciton lines were assigned a Lorentzian band shape with fwhm equal to 2 cm^{-1} for the $k = 0$ transition and 53 cm^{-1} for both the $k = +1$ and $k = -1$ transitions. It was assumed that the dipole strength of the $k = 0$ transition constituted about 3% of the dipole strength of the $k = +1$ and $k = -1$ transitions taken together. The other parameters, the exciton coupling constant, V, and the disorder parameter, $|\Delta/N|$, used to construct the spectrum were $V = 297$ cm^{-1} and $|\Delta/N| = 94$ cm^{-1}.

Evaluation of the Transient Spectra. In a transient absorption experiment, the pump−probe signal is the transient change in probe absorption caused by the pump pulse. As was already mentioned, if optical coherence can be neglected, the pump−probe absorption spectrum can be represented as a sum of GSB, ESA, and SE subspectra. It was demonstrated in ref 32 that a useful insight can be obtained by subtracting the (negative) GSB part from the measured $\Delta OD(\lambda,t)$ spectrum:

$$\Delta OD(\lambda,t) + \sigma_{GSB}(\lambda,t)n(t)d = [\sigma_{ESA}(\lambda,t) - \sigma_{SE}(\lambda,t)]n(t)d \quad (3)$$

In eq 3, $\sigma(\lambda,t)$ with the subscript is the cross section of the corresponding process (GSB, ESA, or SE), $n(t)$ is the concentration of excited molecules at time t, and d is the optical path length. The usefulness of eq 3 stems from the fact that only processes initiating from the excited state contribute to its right-hand part. However, the whole procedure is only feasible when the component spectra and their proportions (i.e., scaling of the

left-hand side ΔOD and $\sigma_{GSB}nd$ terms in eq 3) are known. Moreover, the inhomogeneous broadening of the spectra should not be too large. Otherwise, the transient spectral hole burning (photoselection) overwhelms other effects.

Considering the very different initial shape of the spectra seen in Figures 3 and 5, the presence of the photoselection in our system is obvious. Yet, a qualitative analysis of the spectra and their dependence on the pump wavelength is still possible by modeling different homogeneous one-exciton (and one-exciton to two-exciton) absorption spectra, based on the approximations described in the first part of the Discussion. The homogeneous spectra, like the one in Figure 7, should be convoluted with the instrument spectral response function before using them in simulations of transient absorption spectra. A comparison with the measured spectrum will hopefully tell us whether the approximations and parameters applied were relevant to the problem.

In our simulations, an $N = 9$ circular aggregate of monomeric BChls with the Q_y transition dipoles in the plane of the circle was assumed. The exciton coupling constant was varied between 100 and 400 cm^{-1} and the disorder parameter between 0 and 200 cm^{-1}. Like in Figure 7, exciton transitions were assigned a Lorentzian band shape with fwhm between 1 and 100 cm^{-1}. The instrument spectral response function was approximated by an 8 nm (100−110 cm^{-1}) fwhm Gaussian. Figure 8a presents one of the iterative fitting and decomposition analysis results demonstrating qualitatively satisfying agreement with the experiment.

One of the significant results of the simulation was that exciton coupling and diagonal disorder are almost equally important for the spectral (and dynamic, see below) properties of light excitations in LH2. The shape of the steady-state absorption spectrum can be considered as an incoherent superposition of individual exciton spectra from different B850 rings. The excitons that are (spectrally) less distorted have their partial spectra concentrated around the peak of the overall absorption spectrum. Let us recall that for an undistorted ring the only optically allowed transition is to the degenerate $k = \pm 1$ levels. More distorted excitons have their partial spectra shifted (either to the blue or red) away from the peak of the overall spectrum (see Figure 8b). The larger the shift, the more strongly disturbed is the exciton, and visa versa. Due to symmetry distortion, transitions to the $k = 0$ and $k = >1$ levels gain oscillator strength, as the spectral shift from the (roughly) center of the ground-state absorption spectrum becomes greater. In addition, the degeneracy is removed from the $k = \geq 1$ states, which results in splitting of the levels and the corresponding spectral lines.

Given the above very simplistic model, which in the first order uses only two parameters, the exciton coupling strength and diagonal disorder, the shape of the zero-time transient absorption spectrum and its dependence on excitation wavelength (Figures 3 and 5) can be understood as follows. With the long-wavelength 875 nm excitation, excitons at the red edge of the inhomogeneous distribution (those which are most strongly distorted) are only excited. The selection occurs via the lowest energy $k = 0$ transition that is weakly allowed in distorted rings. The structure of the GSB/SE spectrum observed is due mostly to strong $k = \pm 1$ transitions that are separated because of disorder. Due to relatively low dipole strength, the $k = 0$ transition in Figure 5 does not appear as a separate line, but rather as a shoulder to the lower energy $k = -1$ band (see the model spectrum in Figure 8a). The weak $k = \pm(2-4)$ transitions show up only as a vague structure superimposed on the positive ESA spectrum in Figures 3 and 5. The given interpretation is reinforced by the observation that the spectral position of the ESA shoulder in Figures 3 and 5 follows excitation wavelength. With 865 nm light less distorted excitons get predominantly excited; these excitons have their strong $k = \pm 1$ almost degenerate transition resonant with the excitation pulse. As a result, only a single, relatively narrow GSB/SE band is visible at time zero in Figure 3. Given that excitons even in relatively distorted B850 rings are delocalized at low temperature, it is not only rational but almost the only possibility to explain the subsequent broadening, shifting, and splitting of

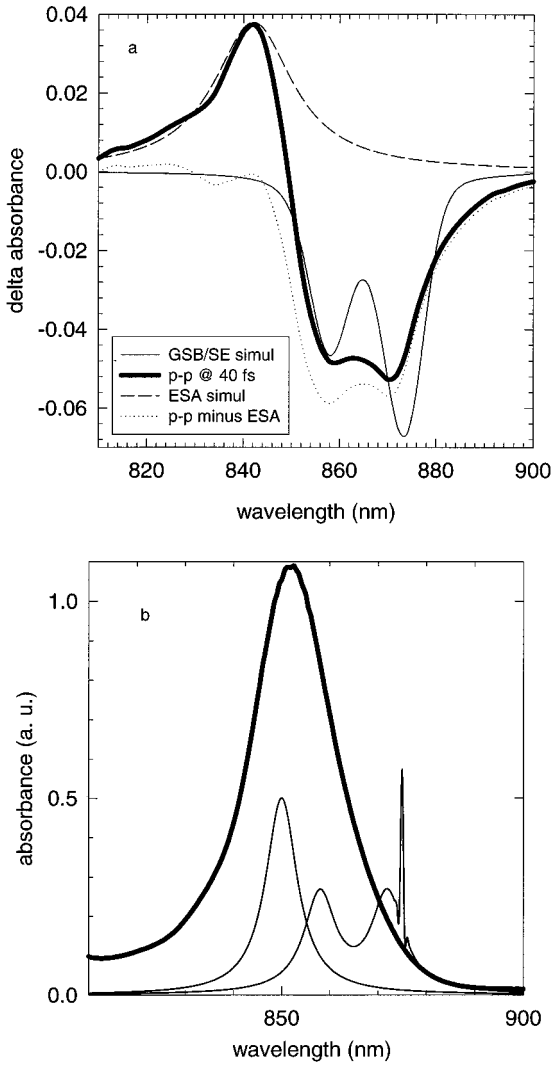

Figure 8. Modeling of the low-temperature experimental spectra. (a) Transient differential absorption spectrum. Highlighted with the bold solid curve is a measured differential absorption spectrum pumped at 875 nm and probed with white light continuum 40 fs after excitation pulse maximum. The dashed ESA simul curve denotes the simulated excited-state absorption spectrum, which was taken a 10 nm fwhm Lorentzian shape. The dotted p−p minus ESA curve is the difference between the experimental pump−probe spectrum and the simulated ESA spectrum. This difference spectrum might give one the idea about the shape of the actual GSB/SE spectrum. The thin solid curve marks the simulated GSB/SE spectrum (see text for the simulation details). (b) Ground-state absorption spectrum. The bold solid curve indicates the experimental B850 absorption band. Shown with thin solid curve are simulated homogeneous spectra of two circular excitons, characterized with different spectral disorder, but of equal total dipole strength. The simulation parameters are similar to the ones used to generate Figure 7. Note that the less disturbed left-hand side exciton has no dipole strength corresponding to the $k = 0$ transition (see text for further details).

the band in terms of exciton energy transfer between different B850 rings in the membrane plane.

Kinetics of the Spectra. In the qualitative framework outlined above, the time-dependent intensity redistribution and decay of pump−probe spectra in Figure 6 can be rationalized as follows. What we have observed is a combined effect of interexciton-state relaxation, exciton energy transfer, and finite exciton lifetime. Considering the large homogeneous width of the $k = \pm 1$ transitions, it is rational to connect the early time dynamics with exciton relaxation. Then, in a reasonable agreement with earlier suggestions,[36−39,45,46] the 800 fs, 15 ps, and 150 ps time constants describe the energy-transfer process. The slowest, about 1 ns time constant, is most probably due to exciton lifetime.[14,39]

The role of exciton relaxation is small with the 875 nm pump (Figure 6b), because almost all excitons get directly excited to their lowest energy $k = 0$ state. A small initial drop of the kinetics measured at 872 nm represents the contribution of exciton relaxation. Energy transfer governs the rest of the dynamics, including the small signal rise after the initial drop. The situation is quite different using 865 nm light (Figure 6a). Now part of the excitons gets pumped to the $k = \pm 1$ levels and another portion to the $k = 0$ state. The fate of the latter excitons is similar to the ones with the 875 nm excitation, except that the number of potential (energetically favorable) acceptors grows vastly (and correspondingly, the energy-transfer rate increases) with higher energy excitation. The excitons that are created via $k = \pm 1$ levels relax within (sub-) 100 fs time to the $k = 0$ state. Due to ultrafast relaxation, these excitons can probably transfer very little energy. The $k = 0$ state carries almost no dipole strength, which means that the excitation energy gets trapped to certain rings and cannot be transferred (at least by the common Forster energy-transfer mechanism).

In terms of transient absorption spectra, one can still "see" the least disturbed "good excitons" following relaxation to the $k = 0$ state, because the GSB is conserved until the exciton is quenched. Interestingly, the more perfect the circular exciton, the longer its lifetime. The spectral and temporal behavior of ESA described in Results section may now also be explained as due to changing overlap of the GSB/SE and ESA subspectra in the course of exciton relaxation and energy transfer.

Parameters. The basic model parameters, exciton coupling constant and disorder parameter, can be readily estimated from the experimental spectra. From Figure 5, the energy separation between the $k = \pm 1$ and $k = 0$ levels can be found as the difference between the midpoint of the split $k = \pm 1$ levels and the pump pulse frequency. Then by using eq 2, V can be calculated. We calculated $V = 325 \pm 10$ cm^{-1}, in reasonable agreement with a theoretical estimate in ref 4. According to the model, two separate tools are available from our experiment in order to estimate the disorder parameter: the splitting between the $k = \pm 1$ levels and the position of the exciton level relative to the steady-state absorption maximum. Using the first tool, we conclude from Figure 5 and taking into account the experience gained by the spectral simulation (Figure 8) that $|\Delta/N| = 74 \pm 10$ cm^{-1}. The second tool gives almost a 2 times larger number, 156 ± 10 cm^{-1}. The most probable cause of this discrepancy is that the first-order theory fails at large Δ/N values. Another possibility is that we are dealing with the motional narrowing effect here,[47] which acts upon strong transitions (like $k = \pm 1$) but leaves weak transitions ($k = 0$) unchanged. The third option is that the absorption maximum of the undisturbed excitons does not necessarily coincide with the peak of the steady-state absorption spectrum, an assumption implicitly made here.

Note Added in Proof. Recently, we performed more realistic numerical calculations of excitons in the nine-member ring of heterodimers extending beyond the applicability of the first-order theory. The results of these calculations suggest much larger exciton coupling constant, $V \approx 600$ cm^{-1}.

5. Concluding Remarks

The proposed model provides simple explanations to a number of other experimental observations in LH2 antennas, not directly considered in this work and so far poorly understood. Our preliminary data with LH1 complexes indicate that the spectroscopic properties of B850 and B875 pigment rings are very similar (to be published elsewhere). We are quite confident that many of the following remarks/conclusions apply very well also for the LH1 antennas.

(i) Asymmetric shape of the B850 (B875) ground-state absorption band with small slopes near the base of the band at low temperature (Figure 1). In the context of the above-described principle of the band formation, as an incoherent superposition of individual asymmetric exciton spectra from different B850 rings (Figure 8b), the shape of the overall spectrum is natural.

(ii) Weak temperature dependence and large width of the B850 (B875) absorption band. According to our model, the fwhm of inhomogeneous distribution function is almost the same as the fwhm of the steady-state absorption spectrum at low temperature and probably changes very little with temperature. A large pressure-induced broadening of the absorption spectrum observed in refs 29, 48, and 49 is probably a result of disorded rings having different pressure shift rates.

(iii) Large Stokes shift between the absorption and emission spectra. All the B850 rings contribute additively to the absorption spectrum, whereas in the emission spectrum only the reddest rings show up.

(iv) Very limited site-selective fluorescence line-narrowing effect.[50] Due to inherent technical limitations of the fluorescence line-narrowing method, emission of only nonresonant rings, secondarily excited via an energy-transfer channel, can be recorded. The secondary spectra are necessarily inhomogeneously broadened.

(v) Emission anisotropy dependence of excitation wavelength (anisotropy is at its upper limit ($\approx$0.4) while exciting at the red edge of the absorption spectrum, but decreases fast to about 0.1 when the excitation is tuned to the blue[42,44,50]). Anisotropy decreases because an increasing number of energy-transfer channels are involved at higher energy excitation. The high value of anisotropy with excitation at the red edge seems, at first sight, to contradict the previous comment (iv). However, it is perhaps reasonable to assume that, at the very edge of the absorption spectrum, the number of energy acceptors is low and only ringsthat have the most favorable (head-to-tail) orientation of transition dipoles contribute to the emission. The orientation-preserving energy transfer does not destroy the anisotropy.

(vi) Wavelength-dependent anisotropy in one-color pump−probe spectra, both at room temperature and at low temperature.[15,30] The observed anisotropy behavior can be rationalized, as mentioned above, by taking into account the pump wavelength-dependent interplay between exciton relaxation and energy transfer.

One of the predictions of the present model is that the characteristic doublet structure of the GSB/SE spectrum (see Figure 5) should emerge also when exciting at the blue side of

the steady-state absorption maximum. This was indeed recently observed in our laboratory. (The data are in the process of analysis and will be presented in our forthcoming paper.)

The proposed model has a serious handicap not taking into account the exciton−phonon coupling. (Recent hole-burning data[7,29] have proved almost no coupling to high-frequency local vibrations.) This, however, does not affect our main reasoning, as long as the dynamical properties of the system are not calculated. The spectral red shift, which could be due to the exciton−phonon coupling, is about 12 cm^{-1}. Exciton−phonon coupling could be responsible for a fraction of the 3 nm GSA/SE band red shift observed with 875 nm excitation (Figure 5) as well.

So far, we have not addressed the question of the exciton coherence and the energy-transfer mechanism in the LH2 antenna. Neither of these questions is trivial per se, as was pointed out in ref 51. According to our model, the issue is further complicated because the exciton mean free path, defined as the exciton dephasing length scale, is probably different in different rings.

Finally, it may be of interest to speculate about functional importance of the spectral inhomogeneity. Besides the trivial fact that more light can be harvested with broader spectra, there may be another, perhaps more fundamental reason, at least in circular LH1/2 antennas. In the ideal ringlike antennas the light would have been trapped in the nonactive $k = 0$ level and would have been irreversibly lost for photosynthesis. This probably has been avoided by natural selection, because the bacteria with disorded antennas had higher survival rate. The exact physical cause of the (spectral) disorder still needs to be studied.

Acknowledgment. The work was performed under the U.S. Department of Agriculture Grant No. 96-35306-3569. A.F. acknowledges a partial support from the Estonian Science Foundation, Grant No. 2271. We wish to thank J. Williams for donation of the *Rb. sphaeroides* strain with the *puf* operon deletion and X. Nguyen for help in sample preparation. We are also grateful to K. Timpmann for sharing his unpublished experimental data on LH2 and T. Pullerits and R. van Grondelle for making available their manuscripts prior to publication (refs 14 and 30). Last, but not least, an anonymous referee is acknowledged for useful corrections and persistent criticism which forced us to evaluate our model more completely. This is publication No. 356 from the Arizona State University Center for the Study of Early Events in Photosynthesis.

References and Notes

(1) McDermott, G.; Prince, S. M.; Freer, A. A.; Hawthornthwaite-Lawless, A. M.; Papiz, M. Z.; Cogdell, R. J.; Isaacs, N. W. *Nature* **1995**, *374*, 517.

(2) Koepke, J.; Hu, X.; Muenke, C.; Schulten, K.; Michel, H. *Structure* **1996**, *4*, 581.

(3) Karrasch, S.; Bullough, P. A.; Ghosh, R. *EMBO J.* **1995**, *14-4*, 631.

(4) Sauer, K.; Cogdell, R. J.; Prince, S. M.; Freer, A.; Isaacs, N. W.; Scheer, H. *Photochem. Photobiol*. **1996**, *64*, 564.

(5) Novoderezhkin, V. I.; Razjivin, A. P. *Photosynth. Res*. **1994**, *42*, 9. Dracheva, T. V.; Novoderezhkin, V. I.; Razjivin, A. P. *FEBS Lett*. **1996**, *387*, 81.

(6) Alden, R. G.; Johnson, E.; Nagarajan, V.; Parson, W. W.; Law, C. J.; Cogdell, R. G. *J. Phys. Chem. B* **1997**, *101*, 4667.

(7) Wu, H.-M.; Rätsep, M.; Lee, I.-J.; Cogdell, R. J.; Small, G. J. *J. Phys. Chem. B* **1997**, *101*, 7654. Wu, H.-M.; Small, G. J. *J. Phys. Chem. B* **1998**, *102*, 888.

(8) Sauer, K.; Austin, A. *Biochemistry* **1978**, *17*, 2011.

(9) Scherz, A.; Parson, W. W. *Photosynth. Res.* **1986**, *9*, 21.

(10) Jimenez, R.; Dikshit, S. N.; Bradforth, S. E.; Fleming, G. R. *J. Phys. Chem.* **1996**, *100*, 6825.

(11) Kumble, R.; Palese, S.; Visschers, R. W.; Dutton, P. L.; Hochstrasser, R. M. *Chem. Phys. Lett.* **1996**, *261*, 396.

(12) Jimenez, R.; van Mourik, F.; Yu, J. Y.; Fleming, G. R. *J. Phys. Chem. B* **1997**, *101*, 7350.

(13) Kennis, J. T. M.; Streltsov, A. M.; Permentier, H.; Aartsma, T. J.; Amesz, J. *J. Phys. Chem.* **1996**, *100*, 2438.

(14) Monshouwer, R.; Abrahamsson, M.; van Mourik, F.; van Grondelle, R. *J. Phys. Chem. B* **1997**, *101*, 7241.

(15) Pullerits, T.; Chachisvilis, M.; Sundström, V. *J. Phys. Chem.* **1996**, *100*, 10787.

(16) Picorel, R.; Lefebvre, S.; Gingras, G. *Eur. J. Biochem.* **1984**, *142*, 305.

(17) Leupold, D.; Stiel, H.; Teuchner, K.; Nowak, F.; Sandner, W.; Ücker, B.; Scheer, H. *Phys. Rev. Lett.* **1996**, *77*, 4675.

(18) Novoderezhkin, V. I.; Razjivin, A. P. *FEBS Lett.* **1995**, *368*, 370.

(19) Xiao, W.; Lin, S.; Taguchi, A. K. W.; Woodbury, N. W. *Biochemistry* **1994**, *33*, 8312.

(20) Abdourakhmanov, I. A.; Danielius, R.; Razjivin, A. P. *FEBS Lett.* **1989**, *245*, 47.

(21) Nagarajan, V.; Alden, R. G.; Williams, J. C.; Parson, W. W. *Proc. Natl. Acad. Sci. U.S.A.* **1996**, *93*, 13774.

(22) Wu, H.-M.; Reddy, N. R. S.; Small, G. J. *J. Phys. Chem. B* **1997**, *101*, 651.

(23) Reddy, N. R. S.; Picorel, R.; Small, G. J. *J. Phys. Chem.* **1992**, *96*, 6458.

(24) Hu, X.; Ritz, T.; Damjanovic, A.; Schulten, K. *J. Phys. Chem. B* **1997**, *101*, 3854.

(25) Visser, H. M.; Somsen, O. J. G.; van Mourik, F.; Lin, S.; van Stokkum, I. H. M.; van Grondelle, R. *Biophys. J.* **1995**, *69*, 1083.

(26) Kumble, R.; Palese, S.; Visschers, R. W.; Dutton, P. L.; Hochstrasser, R. M. *Chem. Phys. Lett.* **1996**, *261*, 396.

(27) Meier, T.; Zhao, Y.; Chernyak, V.; Mukamel, S. *J. Chem. Phys.* **1997**, *107*, 1.

(28) Kühn, O.; Sundström, V. *J. Phys. Chem. B* **1997**, *101*, 3432.

(29) Wu, H.-M.; Rätsep, M.; Jankowiak, R.; Cogdell, R. J.; Small, G. J. *J. Phys. Chem. B* **1997**, *101*, 7641.

(30) Chachisvilis, M.; Kühn, O.; Pullerits, T.; V. Sundström, V. *J. Phys. Chem. B* **1997**, *101*, 7275.

(31) Lin, X.; Murchison, H. A.; Nagarajan, V.; Parson, W. W.; Allen, J. P.; Williams, J. C. *Proc. Natl. Acad. Sci. U.S.A.* **1994**, *91*, 10265.

(32) Freiberg, A.; Lin, S.; Timpmann, K.; Blankenship, R. E. *J. Phys. Chem. B* **1997**, *101*, 7211.

(33) Woodbury, N. W.; Peloquin, J. M.; Alden, R. G.; Lin, X.; Lin, S.; Taguchi, A. K. W.; Williams, J. C.; Allen, J. P. *Biochemistry* **1994**, *33*, 8101.

(34) Peloquin, J. M.; Lin, S.; Taguchi, A. K. W.; Woodbury, N. W. *J. Phys. Chem.* **1995**, *99*, 1349.

(35) van der Laan, H.; Schmidt, Th.; Visschers, R. W.; Visscher, K. J.; van Grondelle, R.; Völker, S. *Chem. Phys. Lett.* **1990**, *170*, 231.

(36) Freiberg, A.; Godik, V. I.; Timpmann, K. In *Progress in Photosynthesis Research*; Biggins, J., Ed.; Martinus Nijhoff: Dordrecht, The Netherlands, 1987; Vol. 1, p 45.

(37) Timpmann, K.; Freiberg, A.; Godik, V. I. *Chem. Phys. Lett.* **1991**, *182*, 617.

(38) Freiberg, A.; Timpmann, K. *J. Photochem. Photobiol. B: Biol.* **1992**, *15*, 151.

(39) Godik, V. I.; Timpmann, K.; Freiberg, A.; Moskalenko, A. A. *FEBS Lett.* **1993**, *327*, 68.

(40) Bergström, H.; Westerhuis, W. H. J.; Sundström, V.; van Grondelle, R.; Niederman, R. A.; Gillbro, T. *FEBS Lett.* **1988**, *233*, 12.

(41) Juzeliunas, G. *Z. Phys. D* **1988**, *8*, 379.

(42) Bolt, J.; Sauer, K. *Biochim. Biophys. Acta* **1979**, *546*, 54.

(43) Borisov, A.; Gadonas, R.; Danielius, R.; Piskarskas, A.; Razjivin, A. *FEBS Lett.* **1982**, *138*, 25.

(44) Kramer, H.; Pennoyer, J.; van Grondelle, R.; Westerhuis, W.; Niedermann, R.; Amesz, J. *Biochim. Biophys. Acta* **1984**, *767*, 335.

(45) Pullerits, T.; Freiberg, A. *Biophys. J.* **1992**, *63*, 879.

(46) Pullerits, T.; Visscher, K. V.; Hess, S.; Sundström, V.; Freiberg, A.; Timpmann, K.; van Grondelle, R. *Biophys. J.* **1994**, *66*, 236.

(47) Knapp, E. W. *Chem. Phys.* **1984**, *85*, 73.

(48) Freiberg, A.; Ellervee, A.; Kukk, P.; Laisaar, A.; Tars, M.; Timpmann, K. *Chem. Phys. Lett.* **1993**, *124*, 10.

(49) Tars, M.; Ellervee, A.; Kukk, P.; Laisaar, A.; Saarnak, A.; Freiberg, A. *Lith. J. Phys.* **1994**, *34*, 320.

(50) Monshouwer, R.; Visschers, R. W.; van Mourik, F.; Freiberg, A.; van Grondelle, R. *Biochim. Biophys. Acta* **1995**, *1229*, 373.

(51) Meier, T.; Chernyak, V.; Mukamel, S. *J. Phys. Chem. B* **1997**, *101*, 7332.